Available online at www.sciencedirect.com
SCIENCE DIRECT®
Applied Geochemistry 21 (2006) 788–801
Applied Geochemistry
www.elsevier.com/locate/apgeochem

Laser ablation multicollector ICPMS determination of $\delta^{11}B$ in geological samples

Massimo Tiepolo [a,*], Claudia Bouman [b], Riccardo Vannucci [a,c], Johannes Schwieters [b]

[a] C.N.R. – Istituto di Geoscienze e Georisorse-Sede di Pavia, via Ferrata 1, I-27100 Pavia, Italy
[b] Thermo Electron (Bremen) GmbH, Finnigan Advanced Mass Spectrometry, Hanna-Kunath-Str. 11, 28199 Bremen, Germany
[c] Dipartimento di Scienze della Terra, Università di Pavia, via Ferrata 1, I-27100 Pavia, Italy

Available online 23 March 2006

Abstract

A method for the in situ single spot $\delta^{11}B$ characterisation of geological materials with laser ablation multicollector ICP mass spectrometry (LA-MC-ICPMS) has been developed. The mass spectrometer was equipped with both Faradays and multiple ion counters. Four samples with different B contents (12–31,400 ppm) and isotopic compositions ($\delta^{11}B$ are between −8.71 and +13.6‰) were analysed. Samples include the B4 tourmaline and 3 MPI-DING glasses (StHs6/80-G, GOR132-G and GOR128-G).

All sources of B isotopic fractionation during the analysis (mass bias, laser-induced isotopic fractionation and detector efficiency drift) have been evaluated and quantified. Instrumental mass bias is the major source of fractionation, altering the original isotopic ratio up to 13%. Fractionation related to laser sampling and transport to the ICP was found to be very low (less than 0.0015% s^{-1}). Fractionation effects due to drift in ion counter efficiencies were found to be significant. Nevertheless, the "standard-sample-standard" bracketing approach could be used to correct for the above fractionation effects using NIST SRM 610 as external standard.

With spot sizes of 60–80 μm in diameter, geologically meaningful results can be achieved on samples containing at least 10 ppm B, i.e., results with precisions that can discriminate between the different reservoirs on Earth. Data obtained with Faraday detectors on NIST SRM 610 and B4 tourmaline show high precision (down to 0.04‰, 1σ) and accuracy. Boron isotope ratios measured in the glass samples using multiple ion counting show significantly higher standard deviations (up to 2.5‰, 1σ), but they are very close to the values that can be expected from counting statistics. No significant variations with spot size or B contents were observed. Most of the values are within 1σ level of the reference values.

The developed method was applied to a series of ashes from Mt. Etna erupted in 1995 having B contents between 14 and 20 ppm. The B isotope compositions of the ashes are between −4.8 and −10.7‰, with a weighted average value of -8.0 ± 1.9‰ (1σ).

1. Introduction

Boron is widely recognised as an important tracer in high and low temperature geochemistry (e.g., Palmer and Swihart, 1996). Since B is

* Corresponding author. Tel.: +39 382 505882; fax: +39 382 505890.
E-mail address: tiepolo@crystal.unipv.it (M. Tiepolo).

0883-2927/$ - see front matter © 2006 Elsevier Ltd. All rights reserved.
doi:10.1016/j.apgeochem.2006.02.014

relatively highly soluble in moderate- to high-temperature aqueous fluids, B mobilisation is expected in all magmatic, geothermal and hydrothermal environments where fluids are involved (Leeman and Sisson, 1996). Boron isotope studies have pointed to the involvement of crustal material in magma genesis (e.g., Chaussidon and Jambon, 1994; Chaussidon and Marty, 1995) and a typical field of application of B isotopes concerns subduction zones, where significant amounts of crustal material are recycled into the mantle (e.g., Palmer, 1991; Ishikawa and Nakamura, 1994). Boron isotopes may thus constrain the origin and the nature of the different fluxes involved in petrogenetic processes. Boron isotope signatures are reported in the δ^{11}B notation, i.e. the variation of the $^{11}B/^{10}B$ ratio relative to the NIST SRM 951 boric acid ($\delta^{11}B‰ = [(^{11}B/^{10}B)_{sample}/(^{11}B/^{10}B)_{NIST\ SRM\ 951}\text{-}1]\times 1000$). One of the latest frontiers in modern geochemistry is a better δ^{11}B characterisation of the different Earth and cosmogenic reservoirs (e.g., Chaussidon and Libourel, 1993; Chaussidon and Jambon, 1994) to improve the understanding of Earth and solar system evolution.

Thermal ionisation mass spectrometry (TIMS) is currently the most widely used technique to measure B isotope composition of silicates (e.g., Spivack and Edmond, 1986; Xiao et al., 1988; Vengosh et al., 1989; Leeman et al., 1991; Hemming and Hanson, 1994; Nakano and Nakamura, 1998; Kasemann et al., 2000; Deyhle, 2001). High levels of precision (around 0.04‰, 2σ) and accuracy are obtained after a complex chemical separation procedure (e.g., Tonarini et al., 1997). Furthermore, TIMS, as a bulk rock technique, provides only large-scale chemical information. Secondary ion mass spectrometry (SIMS), even with instruments equipped with a single collector (e.g., Cameca ims 3f), has been shown to be capable of high quality δ^{11}B data (Chaussidon et al., 1997). Despite the lower level of precision relative to TIMS (around 4‰, 2σ), SIMS has the advantages of minimal sample preparation and very high spatial resolution (few tens μm spot diameter). Significant improvements in precision and overall data quality have recently been obtained with the latest generation high sensitivity ion microprobes equipped with multiple ion counters (e.g., Cameca 1270; Kobayashi et al., 2004).

Over the last few years, accurate and precise in situ isotope determinations have been obtained with laser ablation multicollector ICPMS. However, due to the relatively low sensitivity of conventional ICPMS instruments for light masses, especially when operated using laser ablation sampling (Tiepolo et al., 2005), studies have focused on heavy isotopes and/or isotopes that are highly abundant in the sample. This is the case, for example, for Hf isotopes in zircons (e.g., Griffin et al., 2000, 2002) and Sr isotopes in shells, feldspars or apatites (Christensen et al., 1995; Bizarro et al., 2003). With the exception of a few minerals where B is a major constituent (such as tourmaline), its abundance is usually below 100 ppm and in mantle environments even below 1 ppm (Chaussidon and Marty, 1995). Conventional MC-ICPMS equipped with Faraday detectors requires several hundred ppm B in the samples for a precise determination of the $^{11}B/^{10}B$ ratio, when coupled to a laser ablation system. Using Faraday collectors, the attainable precision on small samples is limited by the noise level of these detectors. Ion counting detectors show much lower noise levels, thereby significantly increasing the signal to noise ratio. The first in situ B isotope measurements with laser ablation MC-ICPMS, substituting the conventional Faraday collectors with more sensitive electron multipliers, were carried out by le Roux et al. (2004). They showed that by rastering relatively large areas of the sample surface (approximately 1 mm × 1 mm) using a laser beam of about 200 μm, accuracies and precisions of 1‰ (2σ) and even lower can be obtained in samples with B contents at the ng/g level. This rastering approach is, however, not suitable for particular petrographic studies where small areas have to be characterised or isotopic disequilibria are expected at the μm scale. Even at the cost of a slightly lower precision, single spot analysis is essential to investigate isotopic variations in mineral zoning patterns, melt pockets or melt inclusions.

Here the results are presented of the first study that assesses the analytical capabilities of LA-MC-ICPMS to produce δ^{11}B data using single spot high spatial resolution (60–80 μm). Faraday detectors were used to analyse a tourmaline (more than 30,000 ppm B). The recently introduced multiple ion counters (MIC) (continuous dynode electron multipliers, Schwieters et al., 2004) were used to analyse a series of glasses with trace levels of B (12–32 ppm). Factors affecting δ^{11}B determinations and major difficulties encountered in the development of the analytical method are described and discussed, and its geological applicability to volcanic ashes is demonstrated.

2. Instrumental and data acquisition

Laser ablation and MC-ICPMS settings and parameters are listed in Table 1. The laser probe used here is the commercially available UP213 from NewWave working at 213 nm. The laser was operated in single spot mode with a repetition rate of 10 Hz and a spot size from 60 to 80 μm in diameter. Laser power was tuned for each sample and spot size in response to the different B contents and matrix behaviours relative to the 213 nm laser radiation. Generally, the laser energy on the sample was in the range 5–20 J/cm^2. Ablation was carried out under He flux in order to reduce fractionation effects and achieve a finer and more homogeneous particulate (Eggins et al., 1998;Günther and Heinrich, 1999). Helium and the ablated material are mixed with Ar downstream of the ablation cell in a T tube.

The Finnigan NEPTUNE (Thermo Electron) MC-ICPMS, equipped with both multiple ion counters and Faraday cups, was used for the detection of B isotopes. The ion counters are identical in size to and interchangeable with the Faraday cups and can replace a Faraday cup, or being attached at the inner and/or outer side of a Faraday cup. In total, up to 9 Faraday cups and 8 ion counting channels can be installed simultaneously on the collector array. In the present configuration, ion counter 5 (IC5) is attached to the outer side of Faraday cup L3 and used for the detection of ^{10}B; IC6 is connected to the outer side of Faraday cup H4 and used for the detection of ^{11}B. Typical peak shapes and peak overlap of ^{10}B and ^{11}B signals are shown in Fig. 1. The ion counters used in this study are so-called channeltrons. Channeltrons tend to produce some after pulses, which could show up 30–40 ns after the main pulse. Therefore, the dead time has been set to 70 ns to avoid any double pulse counting.

First, the instrument was tuned and optimised with solution nebulisation by introducing a Merck B solution (1 μg/mL B). With Faraday detectors, using a double pass spraychamber and a 50 μL/min self-aspirating microconcentric PFA nebuliser, typical sensitivity on ^{11}B was around 4-6 V per μg/mL. Before operating the mass spectrometer with the laser, the ion counters were cross-calibrated by peak jumping the same B signal across the two ion counters involved in the measurements. The ion counter efficiencies were derived by direct comparison of the detector response. The precision of this dynamic peak jumping method very much depends on the signal stability and in order to achieve best precision B was introduced into the ICP by aspirating a very dilute B solution (200 pg/L). Optimal tuning under laser ablation sample introduction was performed before each analytical run using NIST SRM 610 by maximising the ^{11}B signal in response to carrier gas flow (He + Ar) and lens settings. With a spot size of 60 μm and the laser settings reported in Table 1, sensitivity on ^{11}B is about 0.015 mV/

Table 1
Laser and MC-ICPMS operating settings

Laser settings	
Repetition rate	10 Hz
Laser energy	5–20 J/cm^2
Spot size	60–80 μm
ICPMS settings	
Inlet system	
Cool gas (Ar)	15.0 L/min
Auxiliary gas (Ar)	0.65 L/min
Sample gas (Ar)	0.75 to 0.82 L/min
Additional gas (He)	0.68 to 0.76 L/min
X-position	1.46 mm
Y-position	−0.68 mm
Z-position	−2.7 mm
RF power	1200 W
Lenses	
Extraction	−2000 V
Focus	−720 V
X-deflection	1.9 V
Y-deflection	1.6 V
Shape	200 V

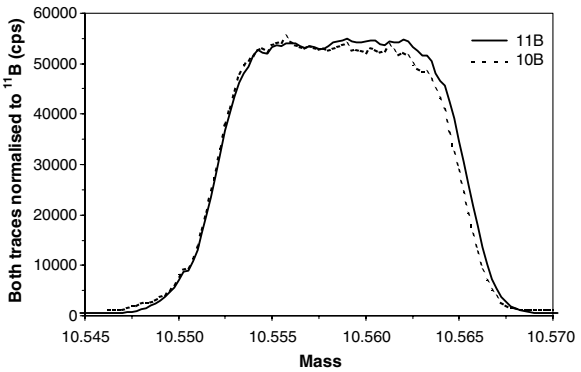

Fig. 1. Overlap and shape of ^{10}B and ^{11}B peaks obtained on ion counters 5 and 6, on the low and high mass side of the collector block. The peaks were obtained using a diluted B solution (natural abundance, 200 ppt). Both traces are normalised to ^{11}B. Due to scattered particles in the lower mass range there are several 100 cps "background" before and after the peaks.

ppm that is approximately a factor of 500,000 times lower than solution nebulisation.

Analyses carried out using Faraday detectors consisted of 30 s baseline acquisition at "half mass position", i.e. before and after the ^{10}B and ^{11}B peaks, followed by 1 block of 90 cycles (1 s integration time/cycle) of laser firing. Analyses carried out using ion counters consisted of 1 block of 120 cycles (1 sec integration time/cycle). During the first 20 cycles the B background was measured (typically ~900 cps ^{11}B). After that, the laser was fired and the B signal was acquired for the remaining 100 s. The net ^{10}B and ^{11}B signals were obtained by subtracting backgrounds from the raw ^{11}B and ^{10}B signals, a so-called "on-peak zero" procedure. The mean $^{11}B/^{10}B$ ratio for each analysis was obtained by averaging 30–40 cycles after signal stabilisation. The remaining data are discharged because count rates become too low. Moreover, this ensures the analysis of just the most superficial layer of the sample. Since the ablation depth is a function of the energy on the sample and the matrix of the ablated material, the depth of the hole drilled cannot be determined without a direct measure with a profilometer. The aspect ratio of 1:1 should however be maintained in the above considered integration interval.

3. Sampling

Four different glass samples spanning from isotopically light B ($\delta^{11}B = -8.71‰$) to heavy B ($\delta^{11}B = +13.5‰$) were analysed (Table 2). Three samples belong to the MPI-DING glass series (Jochum et al., 2000), including StHs6/80-G and the two komatiite glasses GOR132-G and GOR128-G, and have B contents between 11 and 23 ppm (Jochum et al., 2000; Rosner and Meixner, 2004). The two komatiite samples (GOR) differ from the StHs6/80 glass in the significantly lower SiO_2 (45.5 vs. 63.7 wt%) and Na_2O (0.5–0.8 vs. 1.29 wt%) and the higher MgO (22.4 vs. 1.97 wt%) and FeO_T (10.1 vs. 4.37 wt%) contents. The B isotope compositions of these MPI-DING glasses have previously been determined by positive TIMS (Rosner and Meixner, 2004) and are $-4.48 \pm 0.29‰$ (2σ) for StHs6/80-G, $+7.11 \pm 0.97‰$ (2σ) for GOR132 and $+13.6 \pm 0.21‰$ (2σ) for GOR128, respectively. Fragments of about 3×3 mm were selected from each glass, embedded into separate epoxy resin discs and polished down to 1/4 μm of polishing paste. All samples are glassy and no quench crystals at the 10 μm scale have been observed. The fourth sample is the B4 tourmaline, coming from the Rosina pegmatite dyke hosted in the monzogranite of San Piero in Campo, Elba Island (Tonarini et al., 2003). It has a mean B concentration of 31400 ppm. Tonarini et al. (2003) determined a mean $\delta^{11}B$ value of $-8.62 \pm 0.17‰$ (2σ) on milled material and a mean $\delta^{11}B$ value of $-8.85 \pm 0.33‰$ (2σ) on fragments, using positive TIMS. An inter-laboratory comparison of B isotope measurements reported a wide range of $\delta^{11}B$ values between $-7.72‰$ and $-14.66‰$ with a mean value of $-10.3 \pm 2.9‰$ (Gonfiantini et al., 2003).

The NIST SRM 610 glass (National Institute of Standards and Technology Standard Reference Material) is a Si–Na–Ca–Al-oxide glass nominally doped at 500 ppm with a series of trace elements including B (351–363 ppm, Kasemann et al., 2001;NIST website, 1992). The most recent characterisation of NIST SRM 610 for $^{11}B/^{10}B$ is from le Roux et al. (2004) and was obtained with a MC-ICPMS (Axiom) using multiple electron multipliers.

Table 2
B contents and $\delta^{11}B$ signatures of reference samples taken from the literature

	B (ppm)	Reference	$\delta^{11}B$	2σ	Reference
NIST SRM 610	351–363	Kasemann et al. (2001), NIST website (1992)	−0.16/−0.36[a]	0.21/0.06	le Roux et al. (2004)
B4 tourmaline	31,400	Gonfiantini et al. (2003)	−8.71[b]	0.18	Tonarini et al. (2003)
StHs6/80-G	11.6, 12.5	Jochum et al. (2000), Rosner and Meixner (2004)	−4.48[b]	0.29	Rosner and Meixner (2004)
GOR128-G	22.7, 21.8	Jochum et al. (2000), Rosner and Meixner (2004)	+13.55[b]	0.21	Rosner and Meixner (2004)
GOR132-G	17.8, 15.6	Jochum et al. (2000), Rosner and Meixner (2004)	+7.11[b]	0.97	Rosner and Meixner (2004)

[a] Values obtained by MC-ICPMS.
[b] Values obtained by PTIMS.

They reported $^{11}B/^{10}B$ ratios of 4.0494 and 4.0486, corresponding to $\delta^{11}B$ values of −0.16‰ and −0.36‰, relative to NIST SRM 951. In this work the mean value of the previous determinations ($^{11}B/^{10}B = 4.049$) was considered as reference value.

4. Evaluation and correction of isotopic fractionation

Boron has only two stable isotopes. Thus, an internal correction approach cannot be used to approximate isotopic fractionation effects. Furthermore, due to the relatively large mass difference between isotopes in the low mass region (~10% for the two B isotopes), external normalisation on the basis of other known isotopes (e.g., Li or C) is not suitable. Instead, the "standard-sample-standard" bracketing procedure was adopted to correct for isotopic fractionation. This approach has already been successfully adopted by le Roux et al. (2004). NIST SRM 610 was selected as external standard because of its B concentration being within the working range of both ion counters and Faraday detectors. According to the "standard-sample-standard" bracketing procedure, the measured raw $^{11}B/^{10}B$ of the unknown is corrected for isotopic drift to the mean of two bracketing analyses of the NIST SRM 610 reference material and this ratio is further referenced to the average $^{11}B/^{10}B$ ratio (4.049) of NIST SRM 610 taken from le Roux et al. (2004):

$$^{11}B/^{10}B^{\text{corrected}}_{\text{unknown}} = \frac{^{11}B/^{10}B^{\text{measured}}_{\text{unknown}}}{\frac{^{11}B/^{10}B^{\text{measured1}}_{\text{NIST610}} + ^{11}B/^{10}B^{\text{measured2}}_{\text{NIST610}}}{2}} \times \frac{1}{^{11}B/^{10}B^{\text{accepted}}_{\text{NIST610}}}$$

The corrected $^{11}B/^{10}B$ of the unknown is finally referenced to NIST SRM 951 ($^{11}B/^{10}B_{\text{NIST951}} = 4.05003$; Ishikawa and Tera, 1997;Ishikawa et al., 2001) in order to obtain the delta notation. The reliability of the bracketing procedure to correct for isotopic fractionation strongly depends on the agreement between the behaviour of unknown samples and the external standard towards the different sources of isotopic fractionation.

Instrumental mass bias is one of the main sources of isotopic fractionation in ICPMS (e.g., Walczyk, 2003). It is related to space charge effects in the ICP and cone region and it may alter the original isotopic ratio by several percent (Jackson et al., 2001). When dealing with light masses (such as B), due to the large relative mass difference between the isotopes, mass bias effects are even amplified. A first order estimate of mass bias was made by comparing the raw $^{11}B/^{10}B$ ratio, calculated by averaging the first 10 cycles of a laser ablation analysis, with the reference $^{11}B/^{10}B$ ratio of the sample. According to Horn et al. (2000), during the first seconds of ablation, fractionation induced by laser sampling is minimised. In order to eliminate other possible fractionation sources in the instrumental setup, only runs carried out using Faraday detectors were considered. The reference $^{11}B/^{10}B$ ratio of the B4 tourmaline is 4.0151. The mean measured $^{11}B/^{10}B$ value is 4.628, indicating 14% mass bias. Similar percentages of mass bias (13–14%) were obtained on NIST SRM 610, both with Faradays and ion counters. These mass bias values are comparable to those reported by other ICPMS studies (Aggarwal et al., 2003, 2004; le Roux et al., 2004).

Recently, Jackson and Günther (2003) showed that isotopic fractionation is also induced by laser sampling, by transport from the ablation site to the ICP and by the incomplete vaporisation and ionisation of particles in the ICP itself. The preferred mechanism of fractionation seemed to be the evaporation of the lighter isotope during the partial volatilisation of large particles. Jackson and Günther (2003) also showed that by using a high energy density during laser sampling, laser-induced isotopic fractionation is significantly reduced. The extent of laser-induced fractionation on the $^{11}B/^{10}B$ ratio was evaluated on the B4 tourmaline runs and was calculated according to Horn et al. (2000) and Tiepolo et al. (2003) as the variation per second in percent of the $^{11}B/^{10}B$ ratio. Results from the B4 tourmaline reveal that this

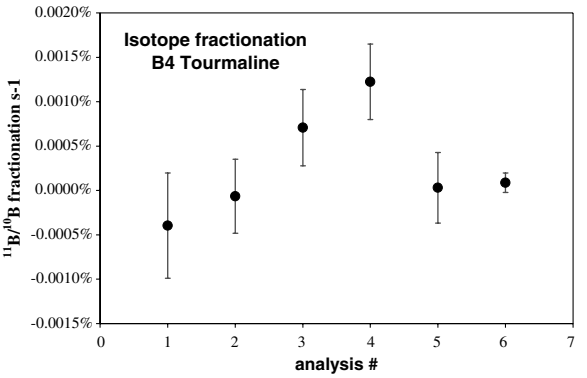

Fig. 2. $^{11}B/^{10}B$ fractionation (% s^{-1}) for B4 tourmaline achieved with a spot size of 60 μm. Signal was collected with Faraday collectors. Error bars are 2σ.

entity of isotopic fractionation is in most cases almost negligible (Fig. 2). The mean value is 0.0003% s^{-1} corresponding to a fractionation of about 0.1‰ per 1 min of ablation. Comparable values were also obtained on the NIST SRM 610 revealing that matrix effects are negligible.

A further source of apparent fractionation of the $^{11}B/^{10}B$ ratio is related to a drift in ion counter efficiencies. For new channeltrons (i.e. the operation voltage is <2000 V), a "burn-in" period is needed for stabilisation of the gain factors. In general, if channeltrons have seen more than 1.5×10^9 counts and have an operation voltage higher than 2300 V the ion counters become more stable. The ion counters used in this study were in the middle of this "burn-in" period, and therefore showed a significant gain drift. Since IC6 (used for the collection of ^{11}B) detects a significantly higher amount of counts compared to IC5 (that detects ^{10}B), the changes in gain drift are more pronounced in IC6 than IC5. The consequence is a decrease of the apparent $^{11}B/^{10}B$ ratio with time, or, to be more precise, with the total amount of counts detected. This drift is linear, as can be seen in Fig. 3, and can thus be corrected by standard-sample-standard bracketing.

The effects of these various sources of fractionation are clearly seen in Fig. 4, which shows that the raw $^{11}B/^{10}B$ ratio linearly decreases with time in both an unknown sample and external standard. The drifts in fractionation for both standard and sample, given by the slope of the two regression lines, are very similar (0.003, Fig. 4). Therefore, the "standard-sample-standard" bracketing procedure using NIST SRM 610 as standard can be used to effectively correct for the fractionation effects.

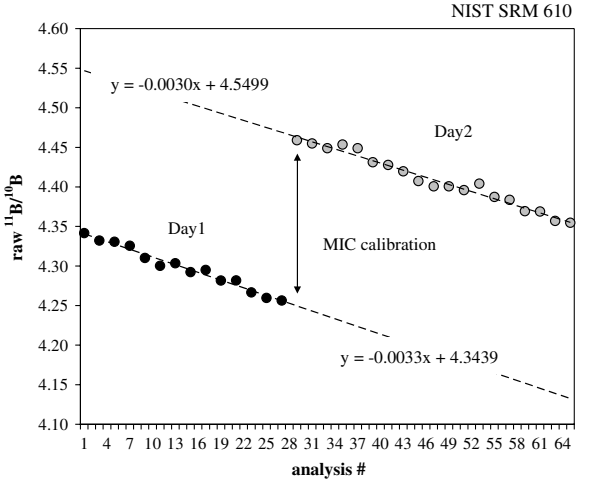

Fig. 3. Day to day variation of the raw $^{11}B/^{10}B$ ratio with analysis number, largely due to drift in ion counter detector efficiencies. The increase in $^{11}B/^{10}B$ from the end of day 1 to the start of day 2 was due to the ion counter calibrations, including operation voltage and efficiency calibrations.

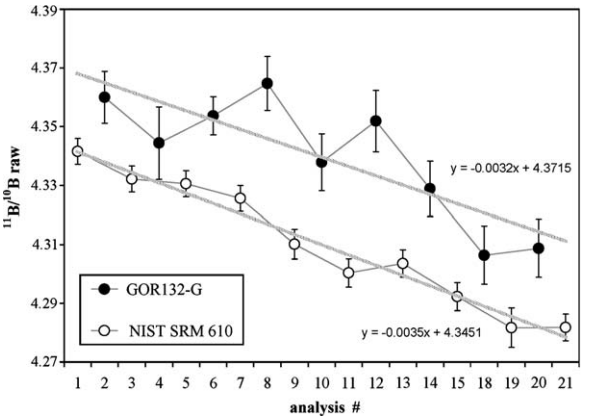

Fig. 4. Variation of the raw $^{11}B/^{10}B$ ratio with analysis number as a consequence of drift in mass fractionation, largely due to drifting ion counter efficiencies. The time interval between the different analyses corresponds approximately to the analysis time (i.e., 2 min).

5. Results

5.1. B4 Tourmaline

The B4 tourmaline was measured using Faraday cups and a spot size of 80 μm. This is the lower limit in spot size dimension for NIST SRM 610 to achieve a reasonable signal for the Faraday detectors. The analytical run consisted of 7 analyses of the NIST SRM 610 standard and 6 analyses of the B4 tourmaline sample. Analyses were randomly performed within the mounted mineral fragment. Results are reported in Table 3 and Fig. 5. The $\delta^{11}B$ values are calculated in two ways: (1) by normalising the sample $^{11}B/^{10}B$ ratio to the mean of the NIST SRM 610 $^{11}B/^{10}B$ data measured before and after the sample, and (2) by normalising the sample $^{11}B/^{10}B$ ratio to the mean of all NIST SRM 610 $^{11}B/^{10}B$ data. The latter is allowed when there is no time-dependent drift. The "standard-sample-standard" bracketing procedure yields a $\delta^{11}B$ value of −8.41 (±0.34‰, 1σ), whereas a value of −8.36 (±0.07‰, 1σ) was obtained by averaging all NIST SRM 610 measurements and using this mean value as normalisation value for the individual analyses of B4. Table 3 shows that the first and the last $^{11}B/^{10}B$ ratios of NIST SRM 610 differ

Table 3
Boron isotope compositions of B4 tourmaline and NIST SRM 610 determined by laser ablation MC-ICPMS (using Faraday detectors)

	$^{11}B/^{10}B$ (measured)	$^{11}B/^{10}B$ (corrected)	1σ	$\delta^{11}B$	1σ
Standard-sample-standard					
B4	4.6268	4.0148	0.0001	−8.70	0.07
B4	4.6276	4.0169	0.0002	−8.19	0.11
B4	4.6269	4.0178	0.0001	−7.97	0.05
B4	4.6272	4.0169	0.0001	−8.19	0.05
B4	4.6274	4.0152	0.0001	−8.59	0.06
B4	4.6270	4.0144	0.0001	−8.80	0.05
Mean value				−8.41	0.34

	$^{11}B/^{10}B$	1σ
Nist610[a]	4.683	0.003
Nist610	4.666	0.002
Nist610	4.663	0.002
Nist610	4.663	0.002
Nist610	4.666	0.002
Nist610	4.667	0.002
Nist610[a]	4.655	0.002

	$^{11}B/^{10}B$ (measured)	$^{11}B/^{10}B$ (corrected)	1σ	$\delta^{11}B$	1σ
By averaging NIST SRM 610 determinations					
B4	4.6268	4.0159	0.0001	−8.42	0.07
B4	4.6276	4.0166	0.0002	−8.25	0.11
B4	4.6269	4.0160	0.0001	−8.40	0.05
B4	4.6272	4.0163	0.0001	−8.34	0.05
B4	4.6274	4.0164	0.0001	−8.29	0.06
B4	4.6270	4.0161	0.0001	−8.38	0.05
Mean value				−8.36	0.07

[a] Not considered (see text).

more than a factor of 2 from the other ratios, and can thus possibly be regarded as outliers. A slight isotopic heterogeneity of the sample or bad ablation conditions due to a momentary instability of the laser system may have caused these offsets. If those NIST SRM 610 analyses are rejected and accordingly the first and last $\delta^{11}B$ values for B4, the "standard-sample-standard" bracketing approach gives a mean $\delta^{11}B$ value for B4 of −8.24 (±0.22‰, 1σ). Thus, the average $\delta^{11}B$ values obtained with the two different approaches of standardisation are statistically indistinguishable suggesting that the "standard-sample-standard" bracketing procedure may not be necessary.

There is an order of magnitude difference in internal precision between the NIST SRM 610 and B4 tourmaline analyses. The relative standard deviation (1σ) on the raw $^{11}B/^{10}B$ ratio for NIST SRM 610 is about 0.5‰, whereas it is down to 0.03‰ for the B4 tourmaline. Reproducibility is estimated to be 0.4‰ for NIST SRM 610 and 0.07‰ for the B4 tourmaline.

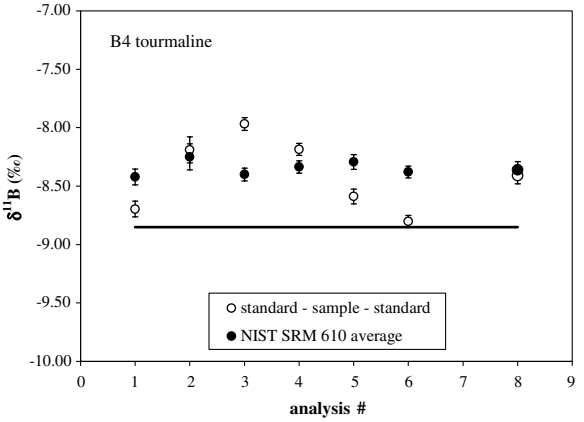

Fig. 5. Boron isotope compositions of B4 tourmaline determined by laser ablation MC-ICPMS (using Faraday detectors and 80 μm spot sizes). Open circles are data obtained by "standard-sample-standard" bracketing using NIST SRM 610 measured before and after the sample. Filled circles are data obtained by normalising against the weighted average NIST SRM 610 ($n = 7$). The black line represents the mean $\delta^{11}B$ value from Tonarini et al. (2003) measured by positive TIMS. Error bars are 2σ.

5.2. MPI-DING glasses

Analyses of MPI-DING glasses were carried out using multiple ion counters. GOR128-G was measured with spot sizes of 60 and 80 μm on separate days. GOR132-G and StHs6/80-G were measured using spot sizes of 60 μm and 80 μm, respectively. Runs of GOR128-G consisted of 8 analyses of sample and 9 analyses of NIST SRM 610. Runs of GOR132-G and StHs6/80 consisted of 9 analyses of sample and 10 analyses of NIST SRM 610. Results are reported in Tables 4–6 and Figs. 6–8. The mean $\delta^{11}B$ values of GOR128-G at 60 and 80 μm spot sizes are statistically equivalent (13.5 ± 1.6‰ and 14.5 ± 2.8‰, respectively). The mean $\delta^{11}B$ values of GOR132-G and StHs6/80-G are 6.8 ± 3.0‰ and -4.3 ± 2.4‰, respectively.

6. Precision and accuracy

The most precise results were obtained on the B4 tourmaline. The errors associated with the average $\delta^{11}B$ value are between 0.1‰ and 0.4‰ and are in good agreement with those obtained by Tonarini et al. (2003) and Gonfiantini et al. (2003) on the same sample using positive TIMS.

Table 4
Boron isotope compositions of MPI-DING glass GOR 128-G and NIST SRM 610 determined by laser ablation MC-ICPMS (using multiple ion counting detectors)

	$^{11}B/^{10}B$ (measured)	$^{11}B/^{10}B$ (corrected)	1σ	$\delta^{11}B$	1σ
60 μm spot size					
GOR128-G	4.540	4.112	0.009	15.3	2.2
GOR128-G	4.524	4.112	0.009	15.3	2.2
GOR128-G	4.491	4.095	0.009	11.1	2.2
GOR128-G	4.487	4.097	0.008	11.7	1.9
GOR128-G	4.488	4.102	0.012	12.9	2.9
GOR128-G	4.486	4.109	0.010	14.5	2.5
GOR128-G	4.489	4.109	0.008	14.6	2.0
GOR128-G	4.481	4.102	0.013	12.8	3.2
Mean value				13.5	1.6

	$^{11}B/^{10}B$	1σ
Nist610	4.481	0.004
Nist610	4.460	0.004
Nist610	4.449	0.003
Nist610	4.432	0.006
Nist610	4.437	0.004
Nist610	4.422	0.005
Nist610	4.420	0.003
Nist610	4.427	0.005
Nist610	4.419	0.004

	$^{11}B/^{10}B$ (measured)	$^{11}B/^{10}B$ (corrected)	1σ	$\delta^{11}B$	1σ
80 μm spot size					
GOR128-G	4.482	4.126	0.012	18.8	2.9
GOR128-G	4.453	4.098	0.010	11.7	2.4
GOR128-G	4.447	4.096	0.009	11.3	2.3
GOR128-G	4.454	4.113	0.006	15.5	1.6
GOR128-G	4.455	4.122	0.008	17.7	2.0
GOR128-G	4.424	4.100	0.009	12.4	2.3
GOR128-G	4.421	4.103	0.008	13.2	2.0
GOR128-G	4.423	4.111	0.007	15.1	1.7
Mean value				14.5	2.8

	$^{11}B/^{10}B$	1σ
Nist610	4.401	0.004
Nist610	4.396	0.005
Nist610	4.404	0.006
Nist610	4.387	0.004
Nist610	4.384	0.003
Nist610	4.369	0.003
Nist610	4.369	0.004
Nist610	4.357	0.004
Nist610	4.355	0.004

The MPI-DING glasses were measured using the multiple ion counting detectors, and show in-run precisions between 1.6‰ and 3.2‰ (1σ, Tables 4–6). They do not show significant variations with spot size (60 and 80 μm) or B contents (11–23 ppm). The precisions obtained on the MPI-DING glasses are significantly lower compared to those commonly achieved

Table 5
Boron isotope compositions of MPI-DING glass GOR 132-G and NIST SRM 610 determined by laser ablation MC-ICPMS (using multiple ion counting detectors)

	$^{11}B/^{10}B$ (measured)	$^{11}B/^{10}B$ (corrected)	1σ	$\delta^{11}B$	1σ
60 μm spot size					
GOR132-G	4.360	4.071	0.009	5.1	2.2
GOR132-G	4.344	4.061	0.012	2.7	3.0
GOR132-G	4.354	4.073	0.006	5.7	1.6
GOR132-G	4.365	4.093	0.009	10.6	2.2
GOR132-G	4.338	4.080	0.010	7.4	2.4
GOR132-G	4.352	4.099	0.011	12.0	2.6
GOR132-G	4.329	4.081	0.009	7.6	2.3
GOR132-G	4.306	4.066	0.010	4.0	2.4
GOR132-G	4.309	4.075	0.010	6.1	2.5
Mean value				6.8	3.0

	$^{11}B/^{10}B$	1σ
Nist610	4.342	0.005
Nist610	4.332	0.004
Nist610	4.331	0.004
Nist610	4.326	0.003
Nist610	4.310	0.005
Nist610	4.300	0.005
Nist610	4.298	0.005
Nist610	4.295	0.007
Nist610	4.282	0.005
Nist610	4.282	0.005

Table 6
Boron isotope compositions of MPI-DING glass StHs6/80 and NIST SRM 610 determined by laser ablation MC-ICPMS (using multiple ion counting detectors)

	$^{11}B/^{10}B$ (measured)	$^{11}B/^{10}B$ (corrected)	1σ	$\delta^{11}B$	1σ
80 μm spot size					
StHs6/80	4.349	4.026	0.010	−5.9	2.4
StHs6/80	4.343	4.031	0.009	−4.7	2.2
StHs6/80	4.331	4.025	0.011	−6.1	2.7
StHs6/80	4.343	4.040	0.012	−2.5	2.9
StHs6/80	4.340	4.036	0.009	−3.5	2.3
StHs6/80	4.305	4.010	0.012	−9.8	3.0
StHs6/80	4.325	4.038	0.010	−2.9	2.6
StHs6/80	4.316	4.037	0.010	−3.2	2.4
StHs6/80	4.323	4.041	0.008	−2.2	2.1
Mean value				−4.3	2.4

	$^{11}B/^{10}B$	1σ
Nist610	4.384	0.005
Nist610	4.364	0.005
Nist610	4.361	0.004
Nist610	4.352	0.006
Nist610	4.354	0.005
Nist610	4.354	0.005
Nist610	4.340	0.007
Nist610	4.333	0.005
Nist610	4.324	0.005
Nist610	4.339	0.004

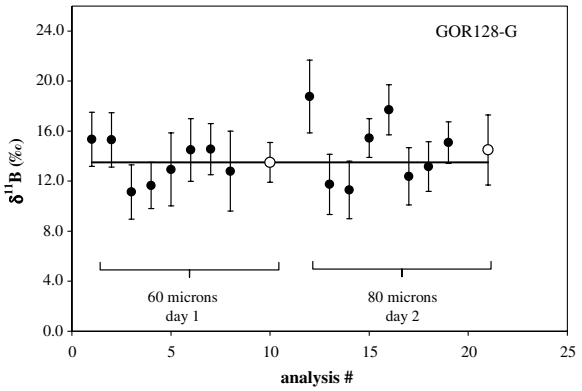

Fig. 6. Boron isotope compositions of GOR128-G determined by laser ablation MC-ICPMS (using multiple ion counting detectors, and 60 and 80 μm spot sizes). Filled circles represent data obtained using the "standard-sample-standard" bracketing approach. Open circles represent weighted average δ^{11}B values. The black line represents the δ^{11}B value from Rosner and Meixner (2004) measured by positive TIMS. Error bars are 2σ.

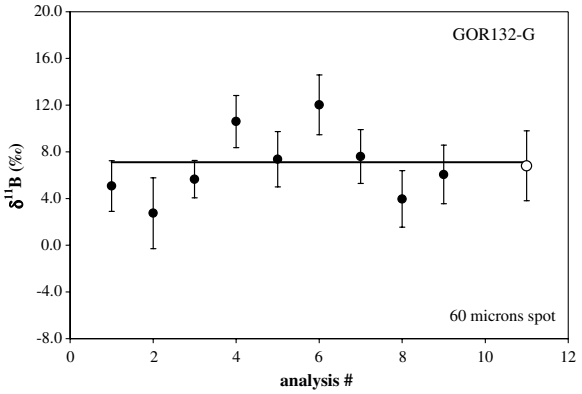

Fig. 7. Boron isotope compositions of GOR132-G determined by laser ablation MC-ICPMS (using multiple ion counting detectors and 60 μm spot sizes). Filled circles represent data obtained using the "standard-sample-standard" bracketing approach. The open circle represents the weighted average δ^{11}B value. The black line represents the δ^{11}B value from Rosner and Meixner (2004) measured by positive TIMS. Error bars are 2σ.

with positive TIMS. For example, on JB-2, a basaltic sample with a similar level of B as the glasses analysed in this work (=30 ppm, Govindaraju, 1994), Tonarini et al. (1997) reported a precision of 0.47‰ (2σ). Errors reported here are also significantly higher (4–5 times) than those reported by le Roux et al. (2004) with a similar instrumental setup. Though, instead of the single spot mode, le Roux et al. (2004) used the raster mode and large sample areas. In both cases, the comparison is not straightforward due to the different detection systems and different spatial resolutions of

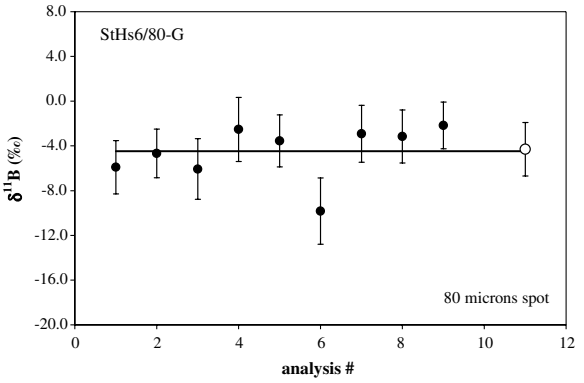

Fig. 8. Boron isotope compositions of StHs6/80 determined by laser ablation MC-ICPMS (using multiple ion counting detectors and 80 μm spot sizes). Filled circles represent data obtained using the "standard-sample-standard" bracketing approach. The open circle represents the weighted average δ^{11}B value. The black line represents the δ^{11}B value from Rosner and Meixner (2004) measured by positive TIMS. Error bars are 2σ.

the techniques, and thus the amount of analysed material. The error on an isotopic ratio (isotope1/isotope2) is a function of the total amount of counts detected. The theoretical best uncertainty achievable is based on Poisson counting statistics, defined as RSD (‰) = $1000 \times \sqrt{(1/N_1 + 1/N_2)}$, where N_1 and N_2 are total amount of counts detected for isotope1 and isotope2 (in the study ^{10}B and ^{11}B), respectively. For signals of 200,000 cps ^{11}B and 50,000 cps ^{10}B (typical for the NIST SRM 610 analyses), a relative uncertainty in the ^{11}B/^{10}B ratio of 1.6‰ is achieved after 10s analysis time. After 40 s analysis time, the theoretical best uncertainty is down to 0.8‰. For the MPI-DING glasses, count rates were lower (~35,000 cps ^{11}B and 8,000 cps ^{10}B) and relative uncertainties of ~2‰ can theoretically be achieved after 40 s analysis time. In practice, uncertainties might be larger due to e.g., signal instability, matrix effects (sample heterogeneity). Here, the relative standard deviations obtained on ^{11}B/^{10}B ratios of the NIST SRM 610 (0.5‰) and the MPI-DING glasses (1.6–3.2‰) are very close to the theoretical values.

The comparison of data precision and accuracy amongst different techniques is not straightforward because results are highly dependent on various parameters, such as degree of homogeneity of the samples, B content, spot size, counting time, and detection system. A rough comparison of the results with those obtained by Secondary Ion Mass Spectrometry (SIMS) shows that the level of precision is comparable. SIMS studies report precisions between 1.5‰ and 3.0‰ (1σ) (Chaussidon and

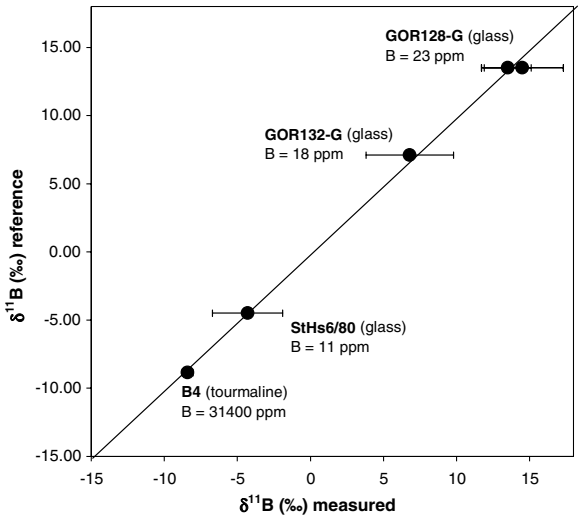

Fig. 9. Comparison between measured and literature (reference) $\delta^{11}B$ values. Literature values come from Tonarini et al. (2003) and Rosner and Meixner (2004). Error bars are 2σ.

Albarède, 1992; Chaussidon and Jambon, 1994; Chaussidon and Marty, 1995; Chaussidon et al., 1997; Straub and Layne, 2002). The SIMS technique, however, possesses a higher spatial resolution compared to laser ablation ICPMS. This is mainly due to the penetration of the ion beam into the sample, which is an order of magnitude less with SIMS than with laser ablation ICPMS.

Data accuracy was assessed on the basis of the weighted average $\delta^{11}B$ values. This is the most appropriate approximation because all $\delta^{11}B$ values of the reference samples have been obtained with bulk rock methods. Fig. 9 shows that the $\delta^{11}B$ results overlap the values from the literature at the 1σ level. The level of accuracy of a single spot analysis is also highly important, because the possibility of reproducing spots in natural samples is not easy. The results show that single spot analyses of B isotopes on the MPI-DING glasses produce $\delta^{11}B$ values that overlap the reference values at the 2σ level. Moreover, more than half of the single spot analyses agree with the reference value at the 1σ level (see Figs. 6–8).

7. Example of application: the $\delta^{11}B$ signature of volcanic ashes

Results obtained in the present work show that the analytical method developed here (laser ablation multiple ion counting ICPMS) can be applied to geological materials when efficient ablation is obtained at the 213 nm laser wavelength. The above reported levels of precision and accuracy are attainable in samples with at least 10 ppm of B and where areas as large as 100 μm can be analysed. The limit of 10 ppm B is too high if the technique needs to be applied to studies of mantle minerals, which, in general, have B contents below the ppm level (Ottolini et al., 2004). Nevertheless, glass pockets and veins in mantle xenoliths and groundmass glasses of mantle-derived lavas and melt inclusions in coexisting phenocrysts may approach or even exceed this concentration limit. Higher B concentrations are relatively common in minerals and glasses from crust-derived materials (Leeman and Sisson, 1996).

To study the applicability of this analytical technique the B isotope composition of volcanic ashes have been characterised. Due to the relatively small dimensions and the large heterogeneity of volcanic ashes (e.g., presence of crystals, lithics and altered portions; Taddeucci et al., 2002), their characterisation using bulk rock methods is extremely challenging and data are difficult to interpret. Ashes, thus, represent a potential field of application of in situ techniques, either for elemental or isotopic analysis. A series of fragments of juvenile fractions of ash erupted in 3 different episodes during the 1995 activity of Mt. Etna have been analysed. A preliminary investigation of ashes under a binocular microscope allowed the selection of glassy clear and crystal-free fragments (Fig. 10). Selected ash fragments were

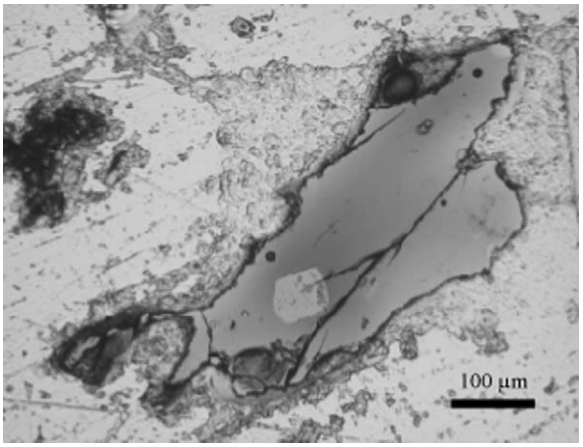

Fig. 10. Photomicrograph in transmitted light of an ash fragment from Mt. Etna embedded into epoxy resin. The ash fragment is constituted by homogeneous and clear glass, the presence of one crystal can be clearly seen in the lower portion of the fragment. All analyses were performed in the clear glass portion.

Table 7
Average major element composition (wt%) of selected ash samples from the 1995 Mt. Etna eruption

	May 9	October 12	December 23
SiO_2	49.51	48.8	48.91
TiO_2	1.96	2.04	1.97
Al_2O_3	16.42	16.37	16.77
Cr_2O_3	0.00	0.02	0.03
FeO	10.25	11.02	10.37
MnO	0.21	0.22	0.23
MgO	3.23	3.44	3.67
CaO	7.14	7.43	7.66
Na_2O	4.81	4.77	4.79
K_2O	3.35	3.62	3.17
	96.88	97.73	97.57

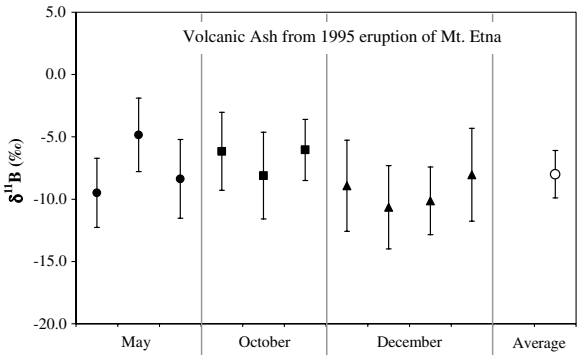

Fig. 11. Boron isotope compositions of ashes erupted during 1995 from Mt. Etna determined by laser ablation MC-ICPMS (using multiple ion counting detectors and 60 μm spot sizes). Filled circles represent data obtained by the ''standard-sample-standard'' bracketing approach. The open circle represents the weighted average $\delta^{11}B$ value. Error bars are 2σ.

mounted in epoxy resin and polished down to 1/4 μm of polishing paste and characterised with electron microprobe (EMP) for major element composition (Table 7). Ten clear portions of glass with dimensions of at least 100 μm were picked for $\delta^{11}B$ analyses (Fig. 11). Preliminary elemental determinations with laser ablation ICPMS (Schiavi et al., 2004) revealed that B concentrations are between 15 and 21 ppm, which is in the range suitable for the analytical technique presented here. Following the approach described above, $\delta^{11}B$ values were determined using NIST SRM 610 as external standard and spot sizes of 60 μm. Table 8 reports $^{11}B/^{10}B$ ratios and $\delta^{11}B$ values of those Mt. Etna ashes. The B isotope compositions range between −4.8 and −10.7‰, with a mean value of -8.0 ± 1.9‰ (1σ). All volcanic ashes overlap at the 2σ level and no statistical difference was observed among the dif-

Table 8
Boron isotope compositions of the volcanic ashes erupted in 1995 from Mt. Etna and NIST SRM 610 determined by laser ablation MC-ICPMS (using multiple ion counting detectors)

	$^{11}B/^{10}B$ (measured)	$^{11}B/^{10}B$ (corrected)	1σ	$\delta^{11}B$	1σ
9-5-95a	4.533	4.012	0.011	−9.5	2.8
9-5-95b	4.519	4.030	0.012	−4.8	3.0
9-5-95c	4.493	4.016	0.013	−8.4	3.2
12-10-95a	4.465	4.025	0.013	−6.2	3.1
12-10-95b	4.439	4.017	0.014	−8.1	3.5
12-10-95c	4.444	4.026	0.010	−6.0	2.5
23-12-95a	4.476	4.014	0.015	−8.9	3.7
23-12-95b	4.460	4.007	0.013	−10.7	3.3
23-12-95c	4.462	4.009	0.011	−10.1	2.7
23-12-95d	4.462	4.017	0.015	−8.0	3.7
Mean value				−8.0	1.9

	$^{11}B/^{10}B$	1σ	
Nist610	4.578	0.007	9-5-95a
Nist610	4.566	0.005	9-5-95a
Nist610	4.537	0.006	9-5-95b
Nist610	4.536	0.006	9-5-95b
Nist610	4.520	0.007	9-5-95c
Nist610	4.532	0.005	9-5-95c
Nist610	4.487	0.004	12-10-95a
Nist610	4.489	0.005	12-10-95b
Nist610	4.476	0.005	12-10-95c
Nist610	4.466	0.005	
Nist610	4.472	0.007	23-12-95a
Nist610	4.461	0.007	23-12-95a
Nist610	4.518	0.007	23-12-95b
Nist610	4.505	0.005	23-12-95b
Nist610	4.502	0.008	23-12-95c
Nist610	4.506	0.005	23-12-95c
Nist610	4.500	0.005	23-12-95d
Nist610	4.487	0.004	23-12-95d

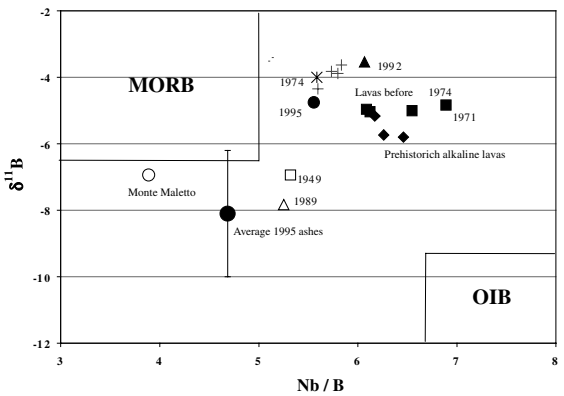

Fig. 12. Comparison between the $\delta^{11}B$ vs. Nb/B ratio of the 1995 ashes and other volcanic products of Mt. Etna. Literature data are from Tonarini et al. (2001).

ferent ash emissions (Fig. 11). The mean $\delta^{11}B$ signature of ashes erupted during 1995 is significantly more negative than those determined on massive volcanic products from the same eruption using bulk techniques (Fig. 12; Tonarini et al., 2001). The ashes also show higher alkali contents ($Na_2O + K_2O = 8.0$ wt%) and lower Nb/B ratios (4.8, Schiavi et al., 2004), compared to the other volcanic products. The compositional decoupling between ashes and massive volcanic products is intriguing and many hypotheses on its origin can be formulated, including e.g., very shallow level contamination related to the hydrothermal system close to the crater vent or B isotopic fractionation as a consequence of degassing. Similar negative $\delta^{11}B$ values were observed for Mt. Maletto and other recent lavas (1949, 1989) and were interpreted as the result of shallow level assimilation of crustal material from the sedimentary pile beneath the volcano (Tonarini et al., 2001). A detailed discussion is beyond the scope of this work and requires more thorough investigations of ashes and other volcanic products.

8. Conclusions

Boron isotope compositions ($\delta^{11}B$) of materials with B contents ranging between 12 and 31,400 ppm have been determined by laser ablation multicollector ICPMS. A New Wave UP213 laser was coupled to a Finnigan Neptune multicollector ICPMS equipped with Faraday and multiple ion counting detectors. The "standard-sample-standard" bracketing approach using NIST SRM 610 was applied to correct for isotopic fractionation.

For samples containing several hundred ppm B, ions were detected using traditional Faraday cups. Faraday detectors are capable of achieving high levels of precision (down to 0.04‰) for in situ B isotope analysis. When B is at the ppm level, the more sensitive ion counting detectors were used to increase the signal to noise ratio. The major limitation in attainable precision are the total amount of counts detected (Poisson counting statistics). Here $\delta^{11}B$ values with precisions down to 1.6‰ are reported. The method is capable of attaining the above levels of precision on samples spanning in composition from tourmaline through komatiite to andesite using the NIST SRM 610 as external standard. The level of accuracy and the relatively large difference in matrix composition within unknown samples and between unknown samples and external standard suggest that for the selected compositions matrix effects are almost negligible.

Application to volcanic ashes demonstrates that valuable results can be obtained and that in situ isotopic analysis may not be comparable with those obtained by bulk rock techniques, opening new frontiers in isotope geochemistry.

Acknowledgement

Klaus Peter Jochum is gratefully thanked for providing the MPI-DING glasses. Massimo Pompilio is gratefully thanked for supplying the ash samples of Mt. Etna. Federica Schiavi is thanked for helping in ash preparation and for major and trace element data of Etna ashes. Sonia Tonarini is acknowledged for providing the B4 tourmaline sample. The manuscript significantly benefited by the reviews of Simone Kasemann, Balz Kamber and Klaus Simon. Funding by CNR-IGG and MIUR (PRIN2003 "In situ isotope analysis of geological materials by Laser Ablation (LA)-ICPMS") are gratefully acknowledged.

References

Aggarwal, J.K., Sheppard, D.S., Mezger, K., Pernicka, E., 2003. Precise and accurate determination of boron isotope ratios by multiple collector ICP-MS: origin of boron in the Ngawha geothermal system, New Zealand. Chem. Geol. 199, 331–342.

Aggarwal, J.K., Mezger, K., Pernicka, E., Meixner, A., 2004. The effect of instrumental mass bias on $\delta^{11}B$ measurements: a comparison between thermal ionisation mass spectrometry and multiple collector ICP-MS. Int. J. Mass Spec. 232, 259–263.

Bizarro, M., Simonetti, A., Stevenson, R.K., Kurszlaukis, S., 2003. In situ $^{87}Sr/^{86}Sr$ investigation of igneous apatites and carbonates using laser-ablation MC-ICP-MS. Geochim. Cosmochim. Acta 67, 289–302.

Chaussidon, M., Albarède, F., 1992. Secular boron isotope variations in the continental crust: an ion microprobe study. Earth Planet. Sci. Lett. 108, 229–241.

Chaussidon, M., Jambon, A., 1994. Boron content and isotopic composition of oceanic basalts: geochemical and cosmochemical implications. Earth Planet. Sci. Lett. 121, 277–291.

Chaussidon, M., Libourel, G., 1993. Boron partitioning in the upper mantle: an experimental and ion probe study. Geochim. Cosmochim. Acta 57, 5053–5062.

Chaussidon, M., Marty, B., 1995. Primitive boron isotope composition of the mantle. Science 269, 383–386.

Chaussidon, M., Robert, F., Mangin, D., Hanon, P., Rose, E.F., 1997. Analytical procedures for the measurement of boron isotope compositions by ion microprobe in meteorites and mantle rocks. Geostand. Newslett. 21, 7–17.

Christensen, J.N., Halliday, A.N., Lee, D.-C., Hall, C.M., 1995. In situ isotopic analysis by laser ablation. Earth Planet. Sci. Lett. 136, 79–85.

Deyhle, A., 2001. Improvements of boron isotope analysis by positive thermal ionization mass spectrometry using static multicollection of $Cs_2BO_2^+$ ions. Int. J. Mass Spectrom. 206, 79–89.

Eggins, S.M., Kinsley, L.P.J., Shelley, J.M.M., 1998. Deposition and elemental fractionation processes during atmospheric pressure laser sampling for analysis by ICPMS. Appl. Surf. Sci. 127, 278–286.

Gonfiantini, R., Tonarini, S., 2003. Intercomparison of Boron Isotope and Concentration measurements. Part II: Evaluation of results. Geostand. Newslett. 27, 41–57.

Govindaraju, K., 1994. 1994 compilation of working values and samples description for 383 geostandards. Geostand. Newslett. 18, 1–158.

Griffin, W.L., Pearson, N.J., Belousova, E., Jackson, S.E., O'Reilly, S.Y., van Achterberg, E., Shee, S.R., 2000. The Hf isotope composition of cratonic mantle: LAM-MC-ICPMS analysis of zircon megacrysts in kimberlites. Geochim. Cosmochim. Acta 64, 133–147.

Griffin, W.L., Wang, X., Jackson, S.E., Pearson, N.J., O'Reilly, S.Y., Xu, X., Zhou, X., 2002. Zircon chemistry and magma mixing, SE China: in-situ analysis of Hf isotopes, Tonglu and Pingtan igneous complexes. Lithos 61, 237–269.

Günther, D., Heinrich, C.A., 1999. Comparison of the ablation behaviour of 266 nm Nd:YAG and 193 nm ArF excimer lasers for LA-ICP-MS analysis. J. Anal. Atom. Spectrom. 14, 1369–1374.

Hemming, N.G., Hanson, G.N., 1994. A procedure for the analysis of boron by thermal ionization mass spectrometry. Chem. Geol. 114, 147–156.

Horn, I., Rudnick, R., McDonough, F., 2000. Precise elemental and isotope ratio determination by simultaneous solution nebulization and laser ablation-ICP-MS: application to U-Pb geochronology. Chem. Geol. 164, 281–301.

Ishikawa, T., Nakamura, E., 1994. Origin of the slab component in arc lavas from across-arc variation of B and Pb isotopes. Nature 370, 205–208.

Ishikawa, T., Tera, F., 1997. Source, composition and distribution of fluid in the Kurile mantle wedge: constraints from across-arc variations of B/Nb and B isotopes. Earth Planet. Sci. Lett. 152, 123–138.

Ishikawa, T., Tera, F., Nakazawa, T., 2001. Boron isotope and trace element systematics of the three volcanic zones in the Kamchatka arc. Geochim. Cosmochim. Acta 65, 4523–4537.

Jackson, S.E., Günther, D., 2003. The nature and sources of laser induced isotopic fractionation in laser ablation-multicollector-inductively coupled plasma-mass spectrometry. J. Anal. Atom. Spectrom. 18, 205–212.

Jackson, S.E., Pearson, N.J., Griffin, W.L., 2001. In situ isotope ratio determination using laser ablation (LA)-magnetic sector-ICP-MS. In: Sylvester, P. (Ed.), Laser Ablation-ICPMS in the Earth Sciences, Short Course Series, Vol. 29. Mineralogical Association of Canada, pp. 105–119.

Jochum, K.P., Dingwell, D.B., Rocholl, A., Stoll, B., Hofmann, A.W., 2000. The preparation and preliminary characterization of eight geological MPI-DING reference glasses for in-situ microanalysis. Geostand. Newslett. 24, 87–133.

Kasemann, S., Erzinger, J., Franz, G., 2000. Boron recycling in the continental crust of the central Andes from the Palaeozoic to Mesozoic, NW Argentina. Contrib. Mineral. Petrol. 140, 328–343.

Kasemann, S., Meixner, A., Rocholl, A., Venemann, T., Rosner, M., Schmitt, A., Wiedebeck, M., 2001. Boron and oxygen isotope composition of certified reference materials NIST SRM 610/612 and certified reference materials JB-2 and JR-2. Geostand. Newslett. 25, 405–416.

Kobayashi, K., Tanaka, R., Moriguti, T., Shimizu, K., Nakamura, E., 2004. Lithium, boron, and lead isotope systematics of glass inclusions in olivines from Hawaiian lavas: evidence for recycled components in the Hawaiian plume. Chem. Geol. 212, 143–161.

Leeman, W.P., Sisson, V.B., 1996. Geochemistry of boron and its implications for crustal and mantle processes. In: Grew, E.S., Anovitz, L.M. (Eds.), Boron: Mineralogy, Petrology and Geochemistry Reviews in Mineralogy. Mineralogical Society of America, Washington, pp. 645–707.

Leeman, W.P., Vocke, R.D., Beary, E.S., Paulsen, P.J., 1991. Precise boron isotopic analysis of aqueous samples: ion exchange extraction and mass spectrometry. Geochim. Cosmochim. Acta 55, 3901–3907.

le Roux, P.J., Shirey, S.B., Benton, L., Hauri, E.H., Mock, T.D., 2004. In situ, multiple-multiplier, laser ablation ICP-MS measurement of boron isotopic composition ($\delta^{11}B$) at the nanogram level. Chem. Geol. 203, 123–138.

Nakano, T., Nakamura, E., 1998. Static multicollection of $Cs_2BO_2^+$ ions for precise boron isotope analysis with positive thermal ionization mass spectrometry. Int. J. Mass Spectrom. 176, 13–21.

NIST website: mailto: www.nist.gov, Certificate of analysis: Standard Reference Materials 610 & 611, 1992.

Ottolini, L., Le Fèvre, B., Vannucci, R., 2004. Direct assessment of mantle boron and lithium contents and distribution by SIMS analyses of peridotite minerals. Earth. Planet. Sci. Lett. 226, 415–432.

Palmer, M.R., 1991. Boron-isotope systematics of Halmahera arc (Indonesia) lavas: Evidence for involvement of the subducted slab. Geology 19, 215–217.

Palmer, M.R., Swihart, G.H., 1996. Boron isotope geochemistry: An overview. In: Grew, E.S., Anovitz, L.M. (Eds.), Boron: Mineralogy, Petrology and Geochemistry Reviews in Mineralogy.. Mineralogical Society of America, Washington, pp. 845–962.

Rosner, M., Meixner, A., 2004. Boron isotopic composition and concentration of ten geological reference materials. Geostand. Geoanal. Res. 28, 431–441.

Schiavi, F., Bouman, C., Corsaro, R., Miraglia, L., Pompilio, M., Tiepolo, M., Vannucci, R., Zanon, V., 2004. In-situ trace element and boron isotopic composition of glassy juvenile fraction of ash of the 1995 summit activity of Mt. Etna. A laser ablation ICP-SFMS and MIC-ICP-MS study. Abstr. Vol. IAVCEI General Assembly 2004, Pucon, Chile.

Schwieters, J.B., Bouman, C., Tuttas, C., Wieser, M., 2004. A new tool for in situ isotopic analysis of small samples: multiple ion counting – ICPMS and – TIMS. Geochim. Cosmochim Acta 68 (Suppl 1), A60.

Spivack, A.J., Edmond, J.M., 1986. Determinations of boron isotope ratios by thermal ionization mass spectrometry of cesium metaborate cation. Anal. Chem. 58, 31–35.

Straub, S., Layne, G.D., 2002. The systematics of boron isotopes in Izu arc front volcanic rocks. Earth Planet. Sci. Lett. 198, 25–39.

Taddeucci, J., Pompilio, M., Scarlato, P., 2002. Monitoring the explosive activity of the July–August 2001 eruption of Mt.

Etna (Italy) by ash characterisation. Geophys. Res. Lett. 29, 8.

Tiepolo, M., Bottazzi, P., Palenzona, M., Vannucci, R., 2003. A laser probe coupled with ICP – doublefocusing sector-field mass spectrometer for in situ analysis of geological samples and U-Pb dating of zircon. Can. Mineral. 41, 259–272.

Tiepolo, M., Zanetti, A., Vannucci, R., 2005. De termination of Li, Be and B at trace level with Laser Ablation – Inductively Coupled Plasma – Sector Field Mass Spectrometry. Geostand. Geoanal. Res. 29, 211–224.

Tonarini, S., Armienti, P., D'Orazio, M., Innocenti, F., 2001. Subduction-like fluids in the genesis of Mt. Etna magmas: evidence from boron isotopes and fluid mobile elements. Earth Planet. Sci. Lett.. 192, 471–483.

Tonarini, S., Pennini, M., Leeman, W.P., 1997. Precise boron isotopic analysis of complex silicate (rock) samples using alkali carbonate fusion and ion-exchange separation. Chem. Geol. 142, 129–137.

Tonarini, S., Pennisi, M., Adomi-Braccesi, A., Dini, A., Ferrara, G., Gonfiantini, R., Wiedenbeck, M., Groning, M., 2003. Intercomparison of boron isotope and concentration measurements. Part I: selection, preparation and homogeneity tests of time Intercomparison materials. Geostand. Newslett. 27, 29–39.

Vengosh, A., Chivas, A.R., McCulloch, J.M., 1989. Direct determination of boron and chlorine isotopic compositions in geological materials by negative thermal-ionization mass-spectrometry. Chem. Geol. 79, 333–343.

Walczyk, T., 2003. TIMS versus multicollector-ICP-MS: coexistence or struggle for survival? Anal. Bioanal. Chem. 378, 229–231.

Xiao, Y.-K., Beary, E.S., Fasset, J.D., 1988. An improved method for the light precision isotopic measurement of boron by thermal ionisation mass spectrometry. Int. J. Mass Spectrom. Ion. Proc. 85, 203–213.